Journal of Nuclear Materials 397 (2010) 27–30

Contents lists available at ScienceDirect

Journal of Nuclear Materials

journal homepage: www.elsevier.com/locate/jnucmat

Neutron diffraction analyses of U–(6–10 wt.%)Mo alloy powders fabricated by centrifugal atomization

Jong Man Park [a], Ho Jin Ryu [a,*], Ki Hwan Kim [a], Don Bae Lee [a], Yoon Sang Lee [a], Jeong Soo Lee [b], Baek Seok Seong [b], Chang Kyu Kim [a], Marilyne Cornen [c]

[a] Advanced Fuel Technology Development Division, Korea Atomic Energy Research Institute, 150 Deokjin-dong, Yuseong, Daejeon 305-353, Republic of Korea
[b] Neutron Science Division, Korea Atomic Energy Research Institute, 150 Deokjin-dong, Yuseong, Daejeon 305-353, Republic of Korea
[c] INSA de Rennes, UMR CNRS 6226 Sciences Chimiques de Rennes/Chimie-Métallurgie, 20 Avenue des Buttes de Coësmes, 35043 Rennes Cedex, France

ARTICLE INFO

Article history:
Received 26 June 2009
Accepted 26 November 2009

ABSTRACT

Lattice parameters of U–(6–10 wt.%)Mo alloy powders fabricated by a centrifugal atomization technique were measured by neutron diffraction analyses. A micro-segregation of Mo at cell boundaries was observed in the centrifugally atomized U–Mo alloy powders with varying Mo content. Lattice parameters of gamma phases decrease linearly with the increasing Mo content. By separating the overlapped diffraction peaks from cell boundaries and cell interior, lattice parameters and Mo contents of each region were calculated. The Mo content at cell boundaries is about 2–5 at.% lower than that in the cell interior and the lattice parameters for the cell boundaries are higher than those for the cell interior of the atomized U–Mo powder.

1. Introduction

U–Mo alloys are considered as the most promising candidate for advanced research reactor fuel because U–Mo alloys exhibited more stable irradiation performance when compared to other high density uranium alloys and compounds, such as U_3Si, U_6Fe and U_6Mn [1]. The γ-U phase of U–Mo alloy annealed below the eutectoid temperature(560 °C) has a tendency to be decomposed into the lamellar structure consisting of α-U and γ'-U_2Mo phases [2]. However, atomized U–Mo alloy powder retains the meta-stable γ phase at room temperature. When the irradiation behaviors of atomized U–Mo powder and comminuted U–Mo powder were compared, the atomized U–Mo alloy showed the smaller size and the lower number density of fission gas bubbles [3]. The stable irradiation behavior of atomized U–Mo can be closely related to a uniform γ phase formed by rapid solidification. While neutron diffraction studies on irradiated U–Mo/Al dispersion fuels are being carried out [4–6], the effects of Mo content on the microstructure of atomized U–Mo powder have not been investigated yet. U–Mo dispersion fuels with Mo content ranging from 6 to 10 wt.% have been irradiated in recent irradiation tests because the composition range is appropriate considering both irradiation stability and uranium density. Therefore, neutron diffraction analyses on powders of U–(6–10 wt.%)Mo alloy prepared by a rotating disk centrifugal atomization process were carried out in order to characterize the microstructural evolution of atomized U–Mo alloy systems with varying Mo content. The objective of this study is to measure the lattice parameters of γ phases in atomized U–Mo alloys with varying Mo content more in detail.

2. Experimental procedures

U–(6–10 wt.%)Mo alloy powders were produced by a centrifugal atomization technique [7]. Depleted uranium lump (99.9 wt.%) and molybdenum lump (99.7 wt.%) were induction melted in a graphite crucible coated with yttria stabilized zirconia and a total weight of charges per each run was 4 kg. The molten metal is heated to a temperature 200 °C higher than the melting point for each alloy composition and fed onto a rotating graphite disk in an argon atmosphere. The morphology and microstructure of U–(6–10 wt.%)Mo alloy powders were characterized by scanning electron microscopy (SEM). Neutron diffraction patterns of U–(6–10 wt.%)Mo alloy powder samples were obtained at room temperature by a 32-detector high resolution powder diffractometer (HRPD) at KAERI. The monochromized neutrons with a wavelength 0.18339 nm were obtained from a Ge(3 3 1) monochrometer. The sample was contained in a cylindrical vanadium can, 8 mm in diameter and 40 mm in height. Neutron diffraction patterns of U–(6–10 wt.%)Mo alloy powders were analyzed by the Rietveld structure refinement using the FullProf program.

* Corresponding author. Tel.: +82 42 868 8845; fax: +82 42 868 8824.
E-mail address: hjryu@kaeri.re.kr (H.J. Ryu).

0022-3115/$ - see front matter © 2009 Elsevier B.V. All rights reserved.
doi:10.1016/j.jnucmat.2009.11.026

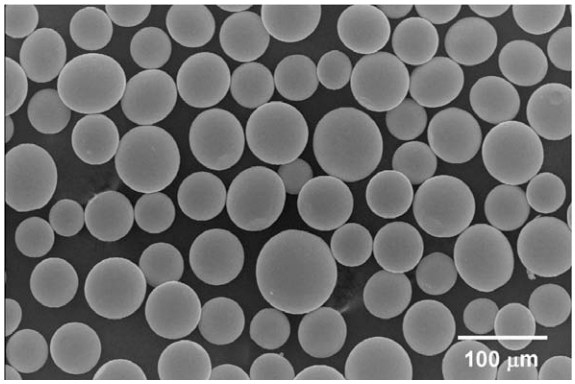

Fig. 1. Scanning electron micrograph of atomized U–10 wt.%Mo powder.

3. Results and discussion

A centrifugally atomized powder appears to be a spherical particle with a smooth surface as represented in Fig. 1. When the chemical composition of U–7 wt.%Mo was analyzed, the difference between the nominal composition and the analyzed composition was not large as shown in Table 1. A cross-sectional micrograph of atomized U–Mo alloy particle after chemical etching was illustrated in Figs. 2 and 3. The thin layer at the periphery of a particle is an oxide layer formed in the atomization chamber by a passivation treatment for prevention from the self ignition of fine uranium alloy powder.

It can be seen that the atomized U–Mo alloy particle has a cell structure with many γ-U cells below 5 μm in size. The cell size becomes smaller as the particle size becomes finer, which indicates that the higher cooling rate of the finer droplet decreases the time available for solidification and thus enhances the finer cell structure [8]. As the Mo concentration increases from 6 to 10 wt.%, the average cell size maintained similar and the cell boundary thickness was about 0.3–0.6 μm. The micro-segregation at cell boundaries of the atomized U–(6–10 wt.%)Mo alloys is due to the solidification characteristics of an alloy with a substantial liquidus–solidus gap. Although a thermodynamic equilibrium assumed in the phase diagram cannot be satisfied in a atomization process since it is a rapid solidification process, the shapes of phase diagram for the solidification of U–Mo alloys (Fig. 4) explain why the cell boundaries have slightly lower Mo concentration when compared with cell interior region [9]. During the solidification of the primary solid phase in the molten metal, the rejection of uranium rich liquid occurs as shown in a U–Mo binary phase diagram. As represented by a tie line at a temperature between the liquidus line and solidus line in Fig. 4, Mo concentration in a solid becomes higher than that in a remaining liquid.

In order to identify the as-quenched phase in atomized U–(6–10 wt.%)Mo alloy powders, neutron diffraction patterns of U–(6–10 wt.%)Mo alloy powders were analyzed. Fig. 5a shows the typical neutron diffraction pattern for atomized U–10 wt.%Mo powder. It appeared that two γ-U phases ($\gamma_{interior}$ and $\gamma_{boundary}$) existed in the atomized U–Mo powders as reported in the previous results [10]. Seong et. al. reported that the atomized U–10 wt.%Mo powder consists of two γ-U solid solution phases having an identical bcc structure, but with slightly different lattice parameters, and accordingly different Mo compositions. Since the two phases ($\gamma_{interior}$ and $\gamma_{boundary}$) with both having Im3m bcc space groups were so similar in unit cell sizes, the peaks of the two phases can be distinguished at higher scattering angles as shown in Fig. 5b.

Table 1
Chemical compositions of an atomized U–7 wt.%Mo alloy.

Elements	U–7 wt.%Mo
Mo (wt.%)	6.97 ± 0.07
Ti (μg/g)	6.0 ± 0.1
Zr (μg/g)	139 ± 3
Cu (μg/g)	25.1 ± 0.4
Ni (μg/g)	81.8 ± 1.2
Fe (μg/g)	177 ± 2
C (μg/g)	50
H (μg/g)	20
O (μg/g)	380
N (μg/g)	70

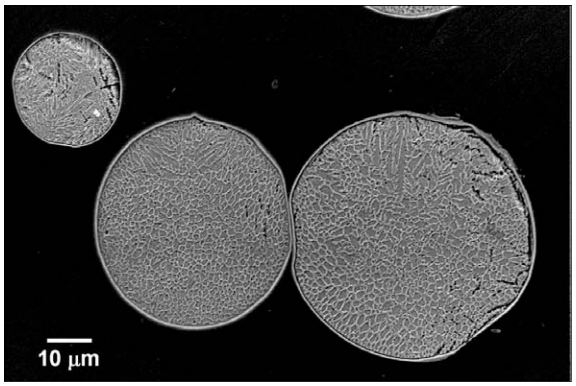

Fig. 2. Scanning electron micrograph of cross-section of atomized U–10wt.%Mo powders (chemically etched).

The lattice parameters of the atomized U–(6–10 wt.%)Mo alloys measured by the neutron diffraction method are listed in Table 2. In case of the U–10 wt.%Mo sample, the lattice constants were a = 0.34112 nm for $\gamma_{interior}$ and a = 0.34261 nm for $\gamma_{boundary}$ phase, respectively. As the Mo concentration increases, the lattice parameters of both the $\gamma_{interior}$ and $\gamma_{boundary}$ phases decrease linearly as shown in Fig. 6 by fitting the data in Table 2. The lattice parameters of the two γ-U phases can be related to the Mo concentration (Mo = 6–10 wt.%) by the following equations obtained by the linear fit;

$$a_o(\text{nm}) = 0.35270 - 0.00119(\text{wt.\%Mo}) \quad \text{for } \gamma_{\text{interior}} \tag{1}$$

$$a_o(\text{nm}) = 0.35299 - 0.00109(\text{wt.\%Mo}) \quad \text{for } \gamma_{\text{boundary}} \tag{2}$$

The standard deviation of the differences of fitted value and measured values was calculated and marked onto the data points in Fig. 6.

The different lattice dimensions are caused by the different Mo concentration. Using the information from an earlier study by Dwight [11], the Mo content of each phase with varying lattice parameters in the U–Mo system can be estimated by the equations as follows:

$$a_o(\text{nm}) = 0.34808 - 0.000314\ (\text{at.\%Mo}) \tag{3}$$

Hence the Mo content is,

$$(\text{at.\%Mo}) = [0.34808 - a_o(\text{nm})]/0.000314 \tag{4}$$

The Mo concentration in the U–10 wt.% Mo solid solutions was calculated to be 22.2 at.% for $\gamma_{interior}$ phase and 17.4 at.% for $\gamma_{boundary}$ phase. The Mo concentrations calculated by Eq. (4) and the

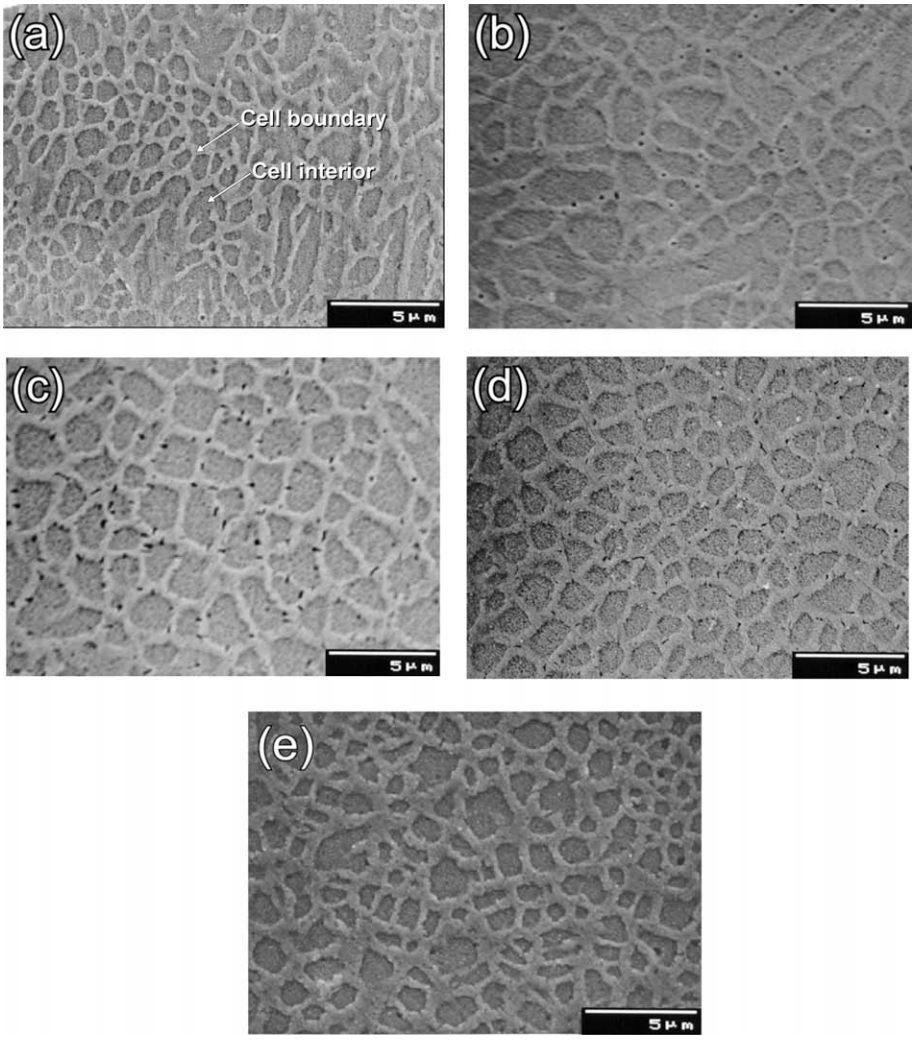

Fig. 3. Cross-sectional SEM images of the atomized U–Mo powders; (a) U–6 wt.%Mo, (b) U–7 wt.%Mo, (c) U–8 wt.%Mo, (d) U–9 wt.%Mo, and (e) U–10 wt.%Mo.

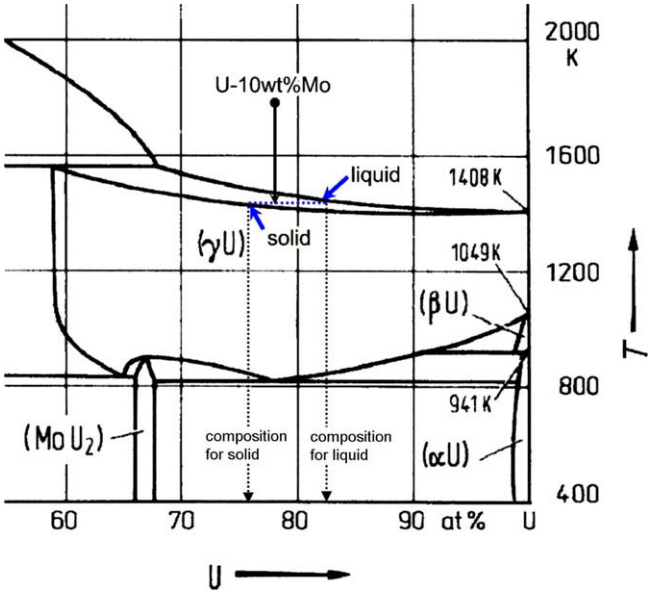

Fig. 4. A partial U–Mo binary phase diagram [9].

measured lattice parameters given in Table 2, were listed in Table 3. The Mo contents at cell boundaries are about 2–5 at.% lower than that in the cell interior, as shown in Table 3.

Solidification microstructures of atomized U–Mo powder affect irradiation performance of U–Mo/Al dispersion fuel. It has been reported that the microstructure of atomized U–Mo shows a cellular appearance after irradiation [3]. Fission gas bubbles first nucleate at cell boundaries, with the lower Mo content, of atomized U–Mo powder. Mo-rich cell interior regions remain as bubble-free areas. Since it has been observed that nano-bubbles are formed in U–Mo during irradiation by transmission electron microscopy [12], bubbles discussed in this study are limited to the bubbles resolvable by SEM.

After a burnup higher than 40 at.% U-235 depletion (based on 19.75% enrichment), irradiation-induced recrystallization occurs primarily at the cell boundaries [13]. Kim et al. showed that the low Mo content in the cell boundaries will stay throughout irradiation [14]. Our measurement data confirmed that the earlier bubble formation and recrystallization at the cell boundaries is associated with the relatively lower Mo content at the cell boundaries in atomized U–Mo powder, because U–Mo alloys with the higher Mo content have more resistance to irradiation damage [3].

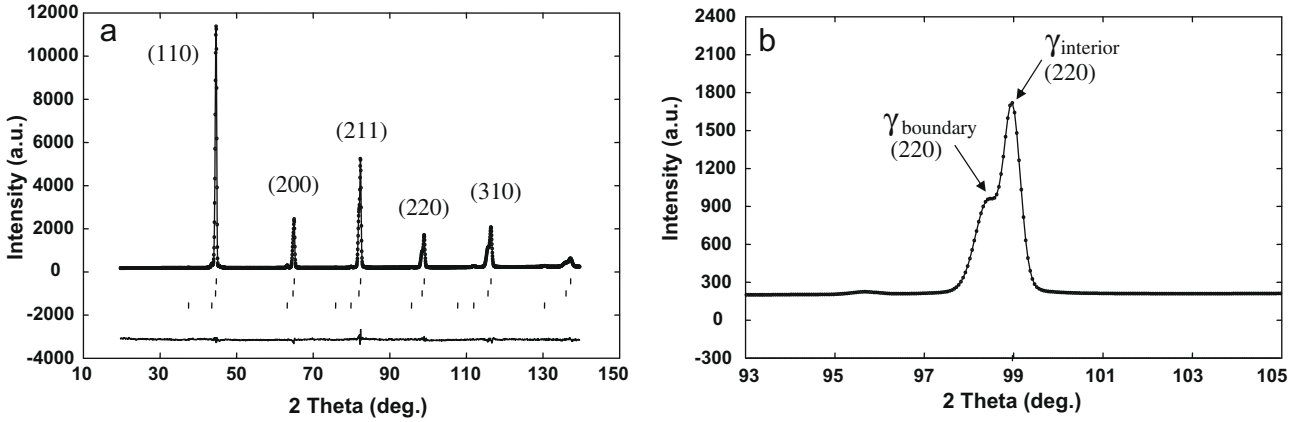

Fig. 5. A neutron diffraction pattern of an atomized U–10 wt.%Mo alloy powder. (a) A whole pattern for wide angles, and (b) overlapped (2 2 0) diffraction peaks for $\gamma_{interior}$-U and $\gamma_{boundary}$-U.

Table 2
Lattice parameters of cell interior ($\gamma_{interior}$) and cell boundaries ($\gamma_{boundary}$) of atomized U–Mo measure by neutron diffraction.

U–Mo Samples	U–6Mo	U–7Mo	U–8Mo	U–9Mo	U–10Mo
Space group	Im3 m	Im3 m	Im3 m	Im3 m	Im3 m
Phase	γ-U	γ-U	γ-U	γ-U	γ-U
a_o (nm)					
$\gamma_{interior}$	0.34546	0.34499	0.34244	0.34164	0.34112
$\gamma_{boundary}$	0.34667	0.34554	0.34365	0.34272	0.34261

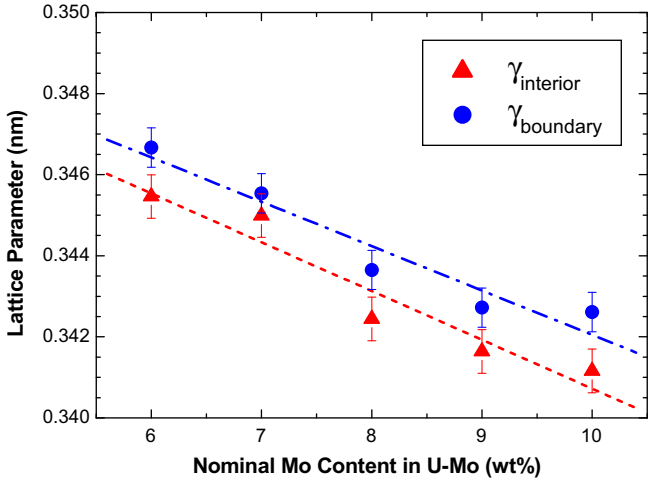

Fig. 6. Lattice parameters of two γ-U phases of atomized U–Mo alloy powders with varying Mo content.

Table 3
Comparison of calculated Mo content by Eq. (4) for cell interior ($\gamma_{interior}$) and cell boundaries ($\gamma_{boundary}$) of atomized U–Mo.

U–Mo samples	U–6Mo	U–7Mo	U–8Mo	U–9Mo	U–10Mo
Mo content calculated by Eq. (4) (at.%)					
$\gamma_{interior}$	8.3	9.8	18.0	20.5	22.2
$\gamma_{boundary}$	4.5	8.1	14.1	17.1	17.4

4. Conclusion

Centrifugally atomized U–(6–10 wt.%)Mo alloy powder exhibits a micro-segregation of Mo at cell boundaries. γ-U phase at cell interior and γ-U phase at the cell boundaries both have a bcc structure, but the Mo content at cell boundaries is about 2–5 at.% lower than that in the cell interior. Lattice parameters of both γ phases at cell interior regions and cell boundaries decrease linearly with the increasing Mo content.

Acknowledgments

The authors would like to express their appreciation to the Ministry of Education, Science and Technology (MEST) of the Republic of Korea for the support of this work through the National Nuclear R&D Project.

References

[1] J.L. Snelgrove, G.L. Hofman, M.K. Meyer, C.L. Trybus, T.C. Wiencek, Nucl. Eng. Design 178 (1997) 119.
[2] R.J. Van Thyne, D.J. McPherson, Trans. ASM 49 (1957) 598.
[3] M.K. Meyer, G.L. Hofman, S.L. Hayes, C.R. Clark, T.C. Wiencek, J.L. Snelgrove, R.V. Strain, K.-H. Kim, J. Nucl. Mater. 304 (2002) 221.
[4] J.S. Lee, C.H. Lee, K.H. Kim, V. Em, J. Nucl. Mater. 280 (2000) 116.
[5] K. Colon, D. Sears, in: Transactions of RRFM-2007, Lyon, France, 11–15 March, 2007.
[6] O.A. Golosov, V.B. Semerikov, A.E. Teplykh, M.S. Lyutikova, E.F. Kartashev, V.A. Lukichev, in: Transactions of RRFM-2007, Lyon, France, 11–15 March, 2007.
[7] C.K. Kim, J.M. Park, H.J. Ryu, Nucl. Eng. Technol. 39 (2007) 617.
[8] K.H. Kim, D.B. Lee, C.K. Kim, G.L. Hofman, K.W. Paik, J. Nucl. Mater. 245 (1997) 179.
[9] T.B. Massalski (Ed.), Binary Alloy Phase Diagrams, ASM International, 1990.
[10] B.S. Seong, C.H. Lee, J.S. Lee, H.S. Shim, J.H. Lee, K.H. Kim, C.K. Kim, V. Em, J. Nucl. Mater. 277 (2000) 174.
[11] A.E. Dwight, J. Nucl. Mater. 2 (1960) 81.
[12] S. Van den Berghe, W. Van Renterghem, A. Leenaers, J. Nucl. Mater. 375 (2008) 340.
[13] G.L. Hofman, Y.S. Kim, Nucl. Eng. Technol. 37 (2005) 299.
[14] Y.S. Kim, G.L. Hofman, J. Rest, G.V. Shevlyakov, ANL Report, ANL-08/11, 2008.